Arabian Journal of Chemistry (2020) **13**, 5363–5376

King Saud University

Arabian Journal of Chemistry

www.ksu.edu.sa
www.sciencedirect.com

ORIGINAL ARTICLE

Synthesis of a new class of corrosion inhibitors derived from natural fatty acid: 13-Docosenoic acid amide derivatives for oil and gas industry

Asma M. Elsharif [a,*], **Samar A. Abubshait** [a], **Ismail Abdulazeez** [b], **Haya A. Abubshait** [c]

[a] *Department of Chemistry, College of Science, Imam Abdulrahman Bin Faisal University, P.O. Box 1982, Dammam 31441, Saudi Arabia*
[b] *Department of Chemistry, King Fahd University of Petroleum and Mineral, Dhahran 31261, Saudi Arabia*
[c] *Department of Basic Science, Deanship of Preparatory Year, Imam Abdulrahman Bin Faisal University, P.O. Box 1982, Dammam 31441, Saudi Arabia*

Received 31 January 2020; accepted 15 March 2020
Available online 24 March 2020

KEYWORDS

Corrosion inhibition;
Mild steel;
Acidic media;
DFT;
13-docosenoic acid amides

Abstract As corrosion inhibitors, a series of new amide derivatives of 13-docosenoic acid was synthesized in yields of above 90% by reacting 13-docosenoic acid with primary and secondary aliphatic and aromatic amines. The inhibition efficiencies (%IEs) of these compounds at various concentrations for the suppression of corrosion of mild steel in 1.00 M HCl exposed for 96 h (4 days) at temperatures in the range 298–333 K were measured via gravimetric corrosion measurements. At 100 ppm, all compounds yielded satisfactory corrosion %IE in 1.00 M HCl; compounds ***2*** and *7* exhibited remarkable %IE of 70.0 and 74.7%, respectively. The results of gravimetric measurements further revealed that compound *7* performed excellently at 60 °C, with %IE = 96.8 at 500 ppm. Quantum chemical density functional theory (DFT) calculations helped predict that compound *7* should have more aromatic character, enabling it to serve as a donor-center for the empty d-orbital of the metal atoms, leading to higher corrosion IE. The adsorption of the inhibitor molecules on the surface of mild steel followed the Langmuir adsorption model, and the free energy of adsorption (ΔG_{ads}) value indicated that the inhibitors are adsorbed through a combined physisorption and chemisorption mechanism to provide effective surface coverage.

* Corresponding author.
E-mail address: aelsharif@iau.edu.sa (A.M. Elsharif).
Peer review under responsibility of King Saud University.

Production and hosting by Elsevier

1. Introduction

Oil fields are generally affected by corrosion and the associated economic loss owing to corrosion of plant systems and piping. Statistical data indicate that corrosion is the main cause of failure of these systems, accounting for 25–30% of the overall

https://doi.org/10.1016/j.arabjc.2020.03.015
1878-5352

losses (Durnie et al., 1999; Bentiss et al., 2000; Sastri, 1998). Numerous approaches are employed for minimization of the wear and corrosion in petroleum plant systems and piping under harsh conditions. One of the most economical approaches for reducing corrosion is the use of corrosion inhibitors (French, 1978; Rosenfeld, 1981; Uhlig and Rivie, 1985; Clewlow et al., 1992). In the industrial context, organic compounds comprising nitrogen, sulfur, and oxygen are extensively employed for acid pickling, descaling, and cleaning, as well as reducing metal corrosion (Sastri, 1998; Revie and Uhlig, 2008; Mernari et al., 1998; Elachouri et al., 2001; Frenier and Growcock, 1993). Chloride ions are highly effective for minimizing the corrosion of mild steel in hydrochloric acid as these ions constrain the corrosion and wear by means of the carbon-based cationic inhibitors (Luo et al., 1998; Fedorov and Morozova, 1987; Putilova et al., 1960). Nevertheless, these inhibitors are not effective in plain H_2SO_4 medium (Murakawa and Hackerman, 1964). This is because the surface charge of iron in both H_2SO_4 and HCl is positive. In the presence of organic compounds, the chloride ions are less readily adsorbed on the mild steel. This is frequently encountered in sulfuric acid solutions but is less pronounced in hydrochloric acid (Rengamani et al., 1994; Bockris and Yang, 1991). This is because the specific adsorption of Cl-, having a low hydration degree, creates $[FeCl\text{-}]_{ads}$, which is anticipated to alter the corrosion potential position E_{corr}, consequently permitting chloride ion adsorption (Antropov, 1963; Lorenz, 1970). In order to prevent iron ions from entering the bulk solution, the creation of a closely-packed layer of $(FeCl\text{-}...Inh^{+})_{ads}$ may minimize the anodic dissolution of iron in hydrochloric acid solution (Morad et al., 1995; Aramaki et al., 1987). It is recognized that the protective features of cations in H_2SO_4 can be enhanced by the addition of halides (Popova et al., 2003). Several effective inhibitors that are efficient for mitigating the corrosion of mild steel in H_2SO_4 and HCl mediums have been reported. Recently, nitrogen-comprising heterocycles and their quaternary salts (Bockris and Yang, 1991), organic compounds comprising isoxazolidine condensation products of amines and carbonyls (Rengamani et al., 1994), aromatic aldehydes (Antropov, 1963), alkenyl phenols (Lorenz, 1970), and diallylammonium moieties (Morad et al., 1995; Aramaki et al., 1987; Popova et al., 2003; Ali et al., 2008a, 2008b, 2003, 2005; Ali and El-sharif, 2012; Ali et al., 2016a, 2016b; El-sharif, 2017; Ali et al., 2012a, 2012b; Frenier et al., 1988; Growcock and Frenier, 1986; Cizek, 1991; Monroe et al., 1963) have been reported as efficient for preventing the corrosion of mild steel in both hydrochloric acid and sulfuric acid solutions. To assess the impact on corrosion inhibition for carbon steel, a range of ethyl esters and ethoxylated fatty acids have been examined (Osman and Shalaby, 2003; Yordanov and Petkov, 2008).

The cationic inhibitors can undergo chemi- or physisorption on the exterior of the metal by displacing surface-adhered water molecules to form a solid obstacle layer (Muralidharan et al., 1995) or by the development of a dative bond through interaction of the non-bonded (lone pair) and p electrons in the inhibitor molecules with the empty d orbitals of the metal (Hackerman and Hurd, 1962). Organic compounds that are normally employed as corrosion inhibitors in oil fields form a protective barrier or film between the corrosive fluids and metal, either owing to their cathodic or anodic behavior, or their mixed behavior (Sanyal, 1981; Revie, 2000).

A continuous determination has been conducted to develop a corrosion inhibitor that exhibits better inhibition at low concentrations in corrosive mediums, while being eco-friendly (Tabatabaei et al., 2020; Bahlakeh et al., 2019; Tabatabaei et al., 2019a; Ramezanzadeh et al., 2019; Dehghani et al., 2019; Tabatabaei et al., 2019b). The present work is devoted to the synthesis of new amides derived from a natural fatty acid (Eurcic acid) and evaluation of these derivatives as potential inhibitors of mild steel corrosion in acid medium. To the best of our knowledge, this is the first report aiming at synthesizing these compounds and studying their corrosion inhibition tendencies.

2. Experimental

2.1. Materials and methods

13-Docosenoic acid (Eurcic acid), phosphoryl chloride, aniline, *o*-anisidine, methylamine, ethylamine, diethylamine, 1-naphthylamine, 3-amino-1,2,4-triazole-5-thiol, and thiophene-2-ethylamine from Sigma Aldrich were used for derivatization of 13-docosenoic acid. A Spectra/Por Standard Regenerated Cellulose (RC) Membrane (Spectrum Laboratories Inc.) was used for dialysis. Dimethyl sulfoxide (DMSO) was dehydrated over calcium hydride overnight and then distilled under decreased pressure at the b.p. of 648–658 °C (4 mm Hg). All solvents were of high-performance liquid chromatography (HPLC) grade. Glass apparatus were washed with distilled or deionized (DI) water. All reactions were performed under nitrogen atmosphere. H_2SO_4 (Fisher Scientific Company), concentrated HCl (A.C.S), and distilled or DI water were used for the acid solutions (1 M). Experiments were performed with the electrolyte solutions in open air using the inhibitor in the concentration range of 0–500 ppm.

2.2. Spectral characterization of inhibitors

Infrared spectrum was recorded on Shimadzu IR-Affinity FTIR spectrometer. ^{13}C NMR and ^{1}H spectra were recorded with a Bruker spectrometer (400 MHZ). The samples were prepared by dissolution of 0.5 ml of sample in 0.6 ml of $CDCl_3$. The chemical shifts (δ) are presented in ppm relative to tetramethylsilane (TMS) as an internal standard. Elemental analysis was conducted with a Carlo-Erba; Elemental analyzer, model 1106.

2.3. Corrosion study

2.3.1. Specimens

The corrosion inhibition tests were conducted by gravimetric measurements in 1.00 M HCl using coupons made from mild steel comprising 99.47% Fe, 0.010% P, 0.005% V, 0.005% Cu, 0.007% Mo, 0.022% Ni, 0.037% Cr, 0.34% Mn, and 0.089% C. For the electrochemical measurement, the test specimen was made in the shape of flag from a mild steel sheet of 1 mm width. The flag base was around 3 cm and insulated with araldite, which is insulating paint. The rest of the area was 1 cm^2, with an exposed area of 2 cm^2. The mild steel specimen

was roughened with emery papers of different grades (grit size of 100, 400, 600, and so on), then de-roughened with propanone and cleaned with distilled or DI water. The specimen was allowed to dry and stored in a desiccator.

2.3.2. Solutions

Solutions of 1.00 M hydrochloric acid were made from concentrated HCl by dilution with deionized water. The inhibitor concentration range was 0–500 ppm. Each corrosion test was conducted with the electrolyte solution in equilibrium.

2.4. Gravimetric measurements

Mild steel specimens, AISI 1018, with dimensions of 2.0 × 2.0 × 0.5 cm were employed for the weight loss corrosion studies. The samples were submerged in 100.0 ml of 1.00 M HCl in the presence and absence of the corrosion inhibitors at varying concentrations (50–500 ppm) and temperatures (298–333 K) for 96 h (4 days). The coupons were cleaned through a process that comprised drying the coupons with a tissue, cleaning with propanone and distilled water, and lastly drying in an oven at 110 °C. Additional weight loss measurements were conducted in the cases where the deviations were higher, in order to attain the anticipated standard deviation (SD). Generally, the coupons were not of the same mass and size; thus, the relative weight loss was employed to compute the percentage inhibition efficiency (%IE), as defined in the methods (Ali et al., 2008a, 2008b, 2003). The mean %IE was found to have a standard deviation of 0.3% to 3.5%. For the inhibitor molecules, the deviation in the higher concentration range was less than 0.5% in 1.00 M HCl. The rate of corrosion was computed by means of Eq. (1) (Zeino et al., 2017; He et al., 2014):

$$CR\ (mmpy) = \frac{8.76 \times 10^4 \times W}{D \times A \times t} \quad (1)$$

where t is the exposure time (h), A is the specimen area (cm^2), D is the density of mild steel (g cm^{-3}), and W is the weight loss (g).

The corrosion inhibition efficiency (η%) and inhibitor surface coverage (θ) were computed by means of Eqs. (2) and (3), respectively:

$$\theta = \left(\frac{CR_o - CR_i}{CR_o}\right) \quad (2)$$

$$\eta\% = \left(\frac{CR_o - CR_i}{CR_o}\right) \times 100 \quad (3)$$

where CR_i and CR_o are rates of corrosion in the presence and absence of the inhibitors. The preliminary weight loss corrosion rate data after 96 h of immersion in 1.00 M HCl in the presence and absence of the corrosion inhibitors are displayed in Fig. 1. The findings showed that compounds ***2*** and ***7*** having one and two aromatic functionalities in their molecular structure, respectively, led to minimal corrosion rates and consequently had higher corrosion inhibition efficiencies and hence were selected for further studies.

2.5. Computational procedure

The molecular geometry of the compounds was fully optimized using density functional theory (DFT) using the B3LYP hybrid functional and 6-31g(d) basis set. The 6-31g(d) basis set was selected as it provides the best estimation of the solvation energies when using an implicit solvent model compared to higher basis sets and often provides good correlation with the experimental results. The 6-31g(d) basis set was selected as it provides the best estimation of solvation energies when using an implicit solvent model compared to higher basis sets and often provides data in good correlation with experimental results (Abdulazeez et al., 2019; Sulaiman and Onawole, 2016). Geometry optimizations and vibrational frequency calculations were conducted to the minima on the potential energy surfaces without imposing any constraints. Reactivity descriptors namely, the energy of the highest occupied molecular orbital (E_{HOMO}), energy of the lowest un-occupied molecular orbital (E_{LUMO}), HOMO-LUMO energy gap (ΔE), electronegativity (χ), global hardness (η), and fraction of electrons transferred during the metal-inhibitor interactions (ΔN) were computed by following DFT-Koopman's theorem, as described elsewhere (Abdulazeez et al., 2019) and summarized in Table S1. To calculate the fraction of transferred electrons, theoretical values of 7.0 eV and 0 were assigned to χ_{Fe} and η_{Fe}, respectively. In order to simulate aqueous medium, Tomasi's polarized continuum model-self consistent reaction field (PCM-SCRF) was adopted with water as the selected solvent (Tomasi et al., 2005). All calculations were conducted with the Gaussian 09 package data extraction (Frisch et al., 2009), visualization, and analysis were accomplished using GaussView 5.0 graphical user interface (Dennington and Millam, 2009).

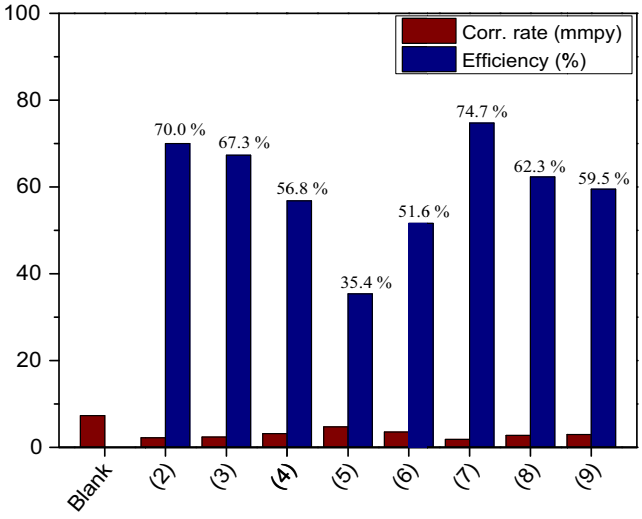

Fig. 1 Weight loss corrosion rates and inhibition efficiencies in 1.00 M HCl in the absence and presence of 100 ppm inhibitor molecules.

2.6. Surface characterization

Field-emission scanning electron microscope (FESEM) analysis was conducted for a mild steel specimen with dimensions of 1.0 × 1.0 × 0.2 cm, immersed in 50 ml of 1.00 M HCl with and without the inhibitors for 24 h. At the end of 24 h, the specimen was rinsed with anhydrous ethanol and deionized water and dried at room temperature. FESEM micrographs were

recorded using a TESCAN LYRA 3 field-emission scanning electron microscope equipped with an energy-dispersive X-ray spectroscope (EDX) detector.

2.7. Synthesis of inhibitors

2.7.1. Part 1: Preparation of Docos-13-enoyl chloride **1**

Dimethylformamide (DMF; 5 ml) in dry benzene and a solution of 13-docosenoic acid (0.5 g, 0.0015 mol) were placed into a one-necked round bottom flask. The flask was equipped with a condenser. A dropping funnel was used to slowly add phosphorus oxychloride ($POCl_3$) to the mixture given the endothermic nature of the reaction. The mixture was stirred for 10 min and heated in oil for 1 h at 90 °C. The mixture was rotary evaporated for 10 min to remove all the solvent. The 13-docosenoyl chloride thus-made was used for additional reaction in the second part.

2.7.2. Part 2: Preparation of 13-docosenoic amides

A primary or secondary aliphatic and aromatic amine, namely (aniline, *o*-anisidine, methylamine, ethylamine, diethyl amine 1-naphthylamine, 3-amino-1,2,4-triazole-5-thiol, and thiophene-2-ethylamine; 0.0015 mol) in dry benzene (30 ml) was placed into a round-bottom flask. A guard tube was used with the flask. A dropping funnel was used to introduce the mixture, which was then stirred for 45 min. When the reflux temperature was reached, the reaction mixture was stirred for 12 h while gradually cooling to room temperature (TLC, *n*-hexane: ethyl acetate, 7:3, *v:v*). The mixture was firstly washed with petroleum ether at 40–60 °C then at 80–100 °C. All solvents were removed and evaporated with a rotary evaporator to afford 13-docosenoic acid amides ***2***, ***3***, ***4***, ***5***, ***6***, ***7***, ***8***, and ***9*** respectively.

*2.7.2.1. Preparation of Docos-13-enoic acid phenyl amide **2**.* Yield (95%), as brown oil. IR (KBr): ν = 2928, 2852, 1435, 1375, 3010, 3022, 1627, 1599, 3324, 1665, 1557 and 1266 cm^{-1}. ^1H NMR, δ: 0.86(t, 3H, —C**H₃**); 1.24–1.33(q, 28H, —CH_2—C**H₂**—CH_2); 1.56(m, 2H, —C**H₂**—CH_2CONH—); 1.98(q, 4H, =CH—C**H₂**—CH_2—); 2.30(t, 2H, —C**H₂**—CONH—); 5.33(t, 2H, —C**H**=C**H**—); 7.00–7.82(m, 5H, =C**H**— Aromatic); 12.25(br, 1H, —N**H**—). ^{13}C NMR, δ: 14.10 (1C, —**C**H_3); 22.69(1C, —**C**H_2—CH_3); 26.52(1C, —**C**H_2—CH_2CO—); 27.22(2C, —**C**H_2—CH=); 29.17–32.61(13C, —**C**H_2—); 34.10 (1C, —**C**H_2—CO—NH); 122.4–130.36(5C, =CH— Ar); 134.38(2C, —**C**H=**C**H—); 170.04(1C, =**C**—NH— Ar); 178.99 (1C, —**C**ONH). $C_{28}H_{47}NO$ (413.37): Calc. %, C, 81.29; H, 11.45; N, 3.87, Found%: C, 81.34; H, 11.40; N, 3.41.

*2.7.2.2. Preparation of Docos-13-enoic acid (2-methoxy phenyl) amide **3**.* Yield (96%) as a light brown oil. IR (KBr): ν = 2922, 2839, 1443, 1332, 3009, 3011, 1630, 1616, 3345, 1742, 1575, 1210 and 1274 cm^{-1}. ^1H NMR, δ: 0.86(t, 3H, —C**H₃**); 1.24–1.33(q, 28H, —CH_2—C**H₂**—CH_2); 1.69(m, 2H, —C**H₂**—CH_2CONH—); 1.94(q, 4H, =CH—C**H₂**—CH_2—); 2.25(t, 2H, —C**H₂**—CONH—); 3.87(s, 3H, —OC**H₃**); 5.87(t, 2H, —C**H**=C**H**—); 6.85–7.37(m, 4H, =C**H** Ar); 11.79(br, 1H, —N**H**—). ^{13}C NMR, δ: 14.10 (1C, —**C**H_3); 22.68(1C, —**C**H_2—CH_3); 25.30(1C, —**C**H_2—CH_2CO—); 27.22(2C, —**C**H_2—CH=); 28.34–32.61(13C, —**C**H_2—); 33.95 (1C, —**C**H_2—CO—NH); 56.05(1C, —O—**C**H_3); 112.27—125.81(4C, =CH— Ar); 128.45(1C, NH—**C**—Ar); 130.00(2C, —**C**H=**C**H—); 154.48(1C, =**C**—OCH_3);172.00 (1C, —**C**ONH). $C_{29}H_{49}NO_2$ (443.38): Calc. %, C, 78.50; H, 11.13; N, 3.16, Found%: C, 78.52; H, 11.15; N, 3.11.

*2.7.2.3. Preparation of Docos-13-enoic acid methyl amide **4**.* 93% yield as a brown oil. IR (KBr): ν = 2919, 2850, 1461, 1366, 3011, 1631, 3340, 1681, 1525 and 1226 cm^{-1}. ^1H NMR, δ: 0.86(t, 3H, —C**H₃**); 1.24–1.33(q, 28H, —CH_2—C**H₂**—CH_2); 1.61(m, 2H, —C**H₂**—CH_2CONH—); 1.99(q, 4H, =CH—C**H₂**—CH_2—); 2.31(t, 2H, —C**H₂**—CONH—); 2.79(s, 3H, —NH—C**H₃**); 5.36(t, 2H, —C**H**=C**H**—); 7.25(br, 1H, —N**H**—). ^{13}C NMR, δ: 14.01 (1C, —**C**H_3); 22.69(1C, —**C**H_2—CH_3); 24.72(1C, —**C**H_2—CH_2CO—); 25.79(1C, —NH—**C**H_3); 27.23(2C, —**C**H_2—CH=); 29.09–32.61(13C, —**C**H_2—); 33.91 (1C, —**C**H_2—CO—NH); 130.30(2C, —**C**H=**C**H—); 179.06 (1C, —**C**ONH). $C_{23}H_{45}NO$ (351.35): Calc. %, C, 78.57; H, 12.90; N, 3.98, Found%: C, 78.60; H, 12.92; N, 4.00.

*2.7.2.4. Preparation of Docos-13-enoic acid ethyl amide **5**.* 95% yield as a brown oil. IR (KBr): ν = 2929, 2843, 1435, 1375, 3010, 1626, 3324, 1731, 1520 and 1200 cm^{-1}. ^1H NMR, δ: 0.86(t, 3H, —C**H₃**); 1.20(s, 3H, —NH—CH_2—C**H₃**); 1.24–1.33 (q, 28H, —CH_2—C**H₂**—CH_2); 1.63(m, 2H, —C**H₂**—CH_2-CONH—); 1.97(q, 4H, =CH—C**H₂**—CH_2—); 2.32(t, 2H, —C**H₂**—CONH—); 3.27(m, 2H, —NH—C**H₂**—); 5.35(t, 2H, —C**H**=C**H**—); 8.6(br, 1H, —N**H**—). ^{13}C NMR, δ: 14.10 (1C, —**C**H_3); 14.85 (1C, —**C**H_3); 22.69(1C, —**C**H_2—CH_3); 25.80 (1C, —**C**H_2—CH_2CO—); 27.22(2C, —**C**H_2—CH=); 29.09–32.70(13C, —**C**H_2—); 34.17 (1C, —**C**H_2—CO—NH); 34.70 (1C, —NH—**C**H_2); 130.36(2C, —**C**H=**C**H—); 179.77 (1C, —**C**ONH). $C_{24}H_{47}NO$ (365.37): Calc. %, C, 78.84; H, 12.96; N, 3.83, Found%: C, 78.79; H,12.93; N, 3.83.

*2.7.2.5. Preparation of Docos-13-enoic acid diethyl amide **6**.* 96% yield as brown oil. IR (KBr): ν = 2924, 2840, 1445, 1377, 3009, 1600, 1742 and 1226 cm^{-1}. ^1H NMR, δ: 0.79(t, 3H, —C**H₃**); 1.18(t, 6H, —NH—CH_2—C**H₃**); 1.29–1.33(q, 28H, —CH_2—C**H₂**—CH_2); 1.55(m, 2H, —C**H₂**—CH_2CONH—); 1.93(q, 4H, =CH—C**H₂**—CH_2—); 2.24(t, 2H, —C**H₂**—CONH—); 3.27(q, 4H, —NH—C**H₂**—); 5.30(t, 2H, —C**H**=C**H**—). ^{13}C NMR, δ: 14.09 (1C, —**C**H_3); 13.07 (2C, —**C**H_3); 22.67(1C, —**C**H_2—CH_3); 24.74(1C, —**C**H_2—CH_2-CO—); 25.59(2C, —**C**H_2—CH=); 29.01–30.90(13C, —**C**H_2—); 32.60 (1C, —**C**H_2—CO—N); 41.36(2C, —N—**C**H_2); 130.3(2C, —**C**H=**C**H—); 172.24 (1C, —**C**ONH). $C_{26}H_{51}NO$ (393.40): Calc. %, C, 70.32; H, 13.06; N, 3.56, Found%: C, 70.35; H, 13.11; N, 3.60.

*2.7.2.6. Preparation of Docos-13-enoic acid naphthalene-1-yl amide **7**.* 97% yield as a brown oil. IR (KBr): ν = 2923, 2853, 1475, 1376, 3011, 1627, 3381, 1741, 1578 and 1227 cm^{-1}. ^1H NMR, δ : 0.86(t, 3H, —C**H₃**); 1.24–1.33(q, 28H, —CH_2—C**H₂**—CH_2); 1.61(m, 2H, —C**H₂**—CH_2CONH—); 1.96(q, 4H, =CH—C**H₂**—CH_2—); 2.33(t, 2H, —C**H₂**—CONH—); 5.36(t, 2H, —C**H**=C**H**—); 7.34–7.86(m, 7H, =CH— Aromatic); 7.93(br, 1H, —N**H**—). ^{13}C NMR, δ : 14.01 (1C, —**C**H_3);

22.69(1C, —**C**H_2—CH_3); 24.27(1C, —**C**H_2—CH_2CO—); 27.30 (2C, —**C**H_2—CH═); 29.85–32.60(13C, —**C**H_2—); 34.01 (1C, —**C**H_2—CO—NH); 109.4–128.3(9C, ═CH— Ar); 132.32(2C, —**C**H═**C**H—); 134.16(1C, ═**C**—NH— Ar); 179.50 (1C, —**C**ONH). $C_{32}H_{49}NO$ (463.38): Calc. %, C, 82.88; H, 10.65; N, 3.45, Found%: C, 82.92; H, 10.63; N, 3.49.

2.7.2.7. Preparation of Docos-13-enoic (5-mercapto-2H-[1,2,4]triazole-3-yl) amide ***8***. Yield (94%) as a yellow oil. IR (KBr): ν = 2916, 2862, 1443, 1357, 3010, 1620, 3270, 3140, 1631, 1515, 1220 and 2540 cm^{-1}. ^{1}H NMR, δ: 0.87(t, 3H, —**C**H_3); 1.24–1.33(q, 28H, —CH_2—**C**H_2—CH_2); 1.63(m, 2H, —**C**H_2—CH_2CONH—); 1.96(q, 4H, ═CH—**C**H_2—CH_2—); 2.34(t, 2H, —**C**H_2—CONH—); 4.20(br, 1H, —**S**H); 5.42(t, 2H, —**C**H═**C**H—); 8.3(br, 2H, —N**H**—). ^{13}C NMR, δ: 14.11 (1C, —**C**H_3); 22.69(1C, —**C**H_2—CH_3); 24.73(1C, —**C**H_2—CH_2-CO—); 27.23(2C, —**C**H_2—CH═); 29.08–32.61(13C, —**C**H_2—); 34.18 (1C, —**C**H_2—CO—NH); 131.7(2C, —**C**H═**C**H—); 142.0 (1C, ═**C**—SH); 148.0(1C, ═**C**—NH—triazole); 172.0 (1C, —**C**ONH). $C_{24}H_{44}N_4OS$ (436.32): Calc. %, C, 66.01; H, 10.16; N, 12.83; S, 7.34, Found%: C, 66.05; H, 10.12; N, 12.85; S 7.32.

2.7.2.8. Preparation of Docos-13-enoic(2-thiophen-2-yl-ethyl)-amide ***9***. 96% yield as a brown oil. IR (KBr): ν = 2920, 2843, 1443, 1377, 3011, 1631, 3320, 1630, 1536 and 1200 cm^{-1}. ^{1}H NMR, δ : 0.86(t, 3H, —**C**H_3); 1.24–1.33(q, 28H, —CH_2—**C**H_2—CH_2); 1.55(m, 2H, —**C**H_2—CH_2CONH—); 1.96(q, 4H, ═CH—**C**H_2—CH_2—); 2.14(t, 2H, —**C**H_2—CONH—); 3.01(t, 2H, —**C**H_2—**C**H_2—NH—); 3.50(t, 2H, —NH—**C**H_2—); 5.33(t, 2H, —**C**H═**C**H—); 6.82—7.14(m, 3H, ═**C**H— thiophene); 7.38(br, 1H, —N**H**—). ^{13}C NMR, δ: 14.30 (1C, —**C**H_3); 22.69 (1C, —**C**H_2—CH_3); 25.70(1C, —**C**H_2—CH_2CO—); 27.68(2C, —**C**H_2—CH═); 29.70–32.94(13C, —**C**H_2—); 34.40 (1C, —**C**H_2-—CO—NH); 32.60(1C, —NH—CH_2—**C**H_2—); 42.9(1C, —NH—**C**H_2—CH_2—); 123.76–126.97 (3C, ═CH— thiophene); 130.37(2C, —**C**H═**C**H—); 141.46(1C, ═C—S— thiophene); 179.21 (1C, —**C**ONH). $C_{28}H_{49}NOS$ (447.35): Calc. %, C, 75.11; H, 11.03; N, 3.13; S, 7.16, Found%: C, 75.10; H, 11.00; N, 3.60; S, 7.20.

3. Results and discussion

3.1. Characterization of 13-docosenoic amides

The new amide derivatives ***2***, ***3***, ***4***, ***5***, ***6***, ***7***, ***8***, and ***9*** were prepared in excellent yields from low-cost materials: aniline, *o*-anisidine, methylamine, ethylamine, diethyl amine 1-naphthylamine, 3-amino-1,2,4-triazole-5-thiol, and thiophene-2-ethylamine, respectively, with 13-docosenoic acid, as shown in Schemes 1, 2, and 3.

The FTIR spectra of compounds ***2***, ***3***, ***4***, ***5***, ***6***, ***7***, ***8***, and ***9*** show bands in the regions of 2915–2930 and 2840–2855 cm^{-1} corresponding to C—H stretching and bands at 3010–3025 and 1600–1630 cm^{-1} for ═C—H, C═C aromatic, and alkene stretching, respectively. New amide bands appeared in the regions of 1630–1740 and 3320–3380 cm^{-1} for —C═O and N—H, respectively. The profile of compound ***6*** showed no N—H amide stretching in this region. A new band appeared at 1210 cm^{-1} due to the methoxy group for compound ***3***. Furthermore, the ^{1}H NMR spectra of the amide derivatives ***2***, ***3***, ***4***, ***5***, ***6***, ***7***, ***8***, and ***9*** showed major signals for **(—CH_3)** at δ 0.79–0.87; (—CH_2—CONH) at δ 2.14–2.34; (—CH_2—CH_2—CH_2—) at δ 1.24–1.33; (═CH—CH_2CH_2—) at δ 1.93–1.99; (CH_2CH_2CONH—) at δ 1.55–1.69; (—CH═CH—) at δ 5.33–5.78; and (br, —NH—) at δ 7.25–12.25. Compounds ***2***, ***3***, and ***7*** showed new aromatic protons (═CH— Ar) at δ 6.85–7.86. Moreover, compound ***6*** showed a signal of (—NH—CH_2—) at δ 3.27. New signals appeared at δ 3.01, 3.50, and 7.38 for (—CH_2—CH_2—NH—), (—NH—CH_2—), and (br, —SH), respectively, for compound ***9***. The ^{13}C NMR spectra of ***2***, ***3***, ***4***, ***5***, ***6***, ***7***, ***8***, and ***9*** presented major carbon signals at δ 13.07–14.30 corresponding to (—CH_3). Signals were also observed at δ 22.67–22.69 (CH_2-—CH_3); δ 24.27–26.52 (—CH_2—CH_2CO—); δ 25.59–27.68 (—CH_2—CH═); δ 28.34–32.94 (13C, —CH_2—); δ 32.60–33.91 (—CH_2—CO—NH); δ 172.01–179.50 (1C, —CONH); and δ 130.00–134.38 (—CH═CH—). New signals appeared at δ 25.79, 34.70, and 41.36 corresponding to (1C, —NH-CH_3), (1C, —NH—CH_2), and (2C, —N—CH_2) for compounds ***4***, ***5***, and ***6***, respectively. Compound ***3*** showed a methoxy signal at δ 56.05 for (—O—CH_3) and a signal at δ 154.48 for (═C—OCH_3). Furthermore, the compounds showed aromatic carbon signals at 109.4–130.36 for (═CH— Ar) and 128.45–170.04 to (═C—NH— Ar) for compounds ***2***, ***3***, and ***7***. Compound ***8*** showed signals at δ 142.0 and 148.0 for (1C, ═C—SH) and (1C, ═C—NH—triazole), respectively. On the other hand, compound ***9*** presented major signals at δ 32.60, 42.90, 123.76–126.97, and 141.46 for (1C, —NH—CH_2—CH_2-—) and at 42.9 (1C, —NH—CH_2—CH_2—), 123.76–126.97 (3C, ═CH— thiophene), and (1C, ═C—S— thiophene). The results of preliminary weight loss corrosion rate measurement after 96 h of immersion of mild steel in 1.00 M HCl in the absence and presence of the inhibitors ***2***, ***3***, ***4***, ***5***, ***6***, ***7***, ***8***, and

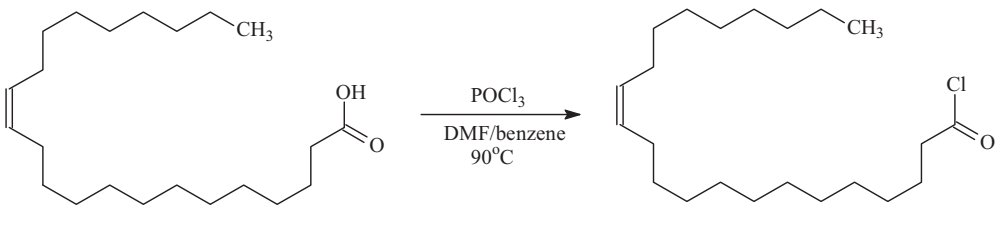

(1)

Scheme 1 Schematic diagram of synthesis of acid chloride **(1)**.

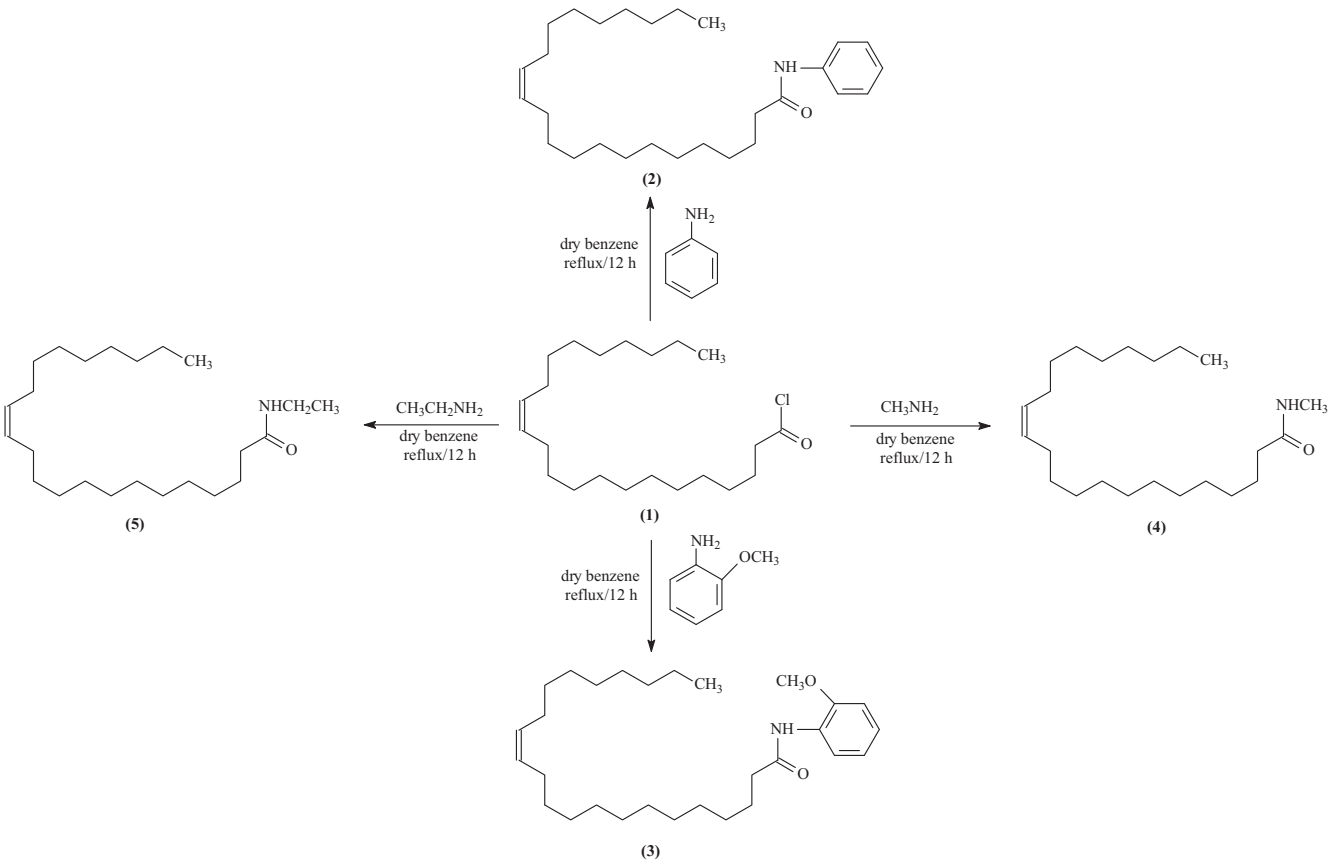

Scheme 2 Schematic diagram of synthesis of acid amide derivatives **(2–5)**.

9 are presented in Fig. 1. The results reveal that in the presence of molecules ***2*** and *7* having one and two aromatic functionalities in their molecular structure, the corrosion rate of the mild steel was minimal, indicative of higher corrosion inhibition efficiencies. Hence, these species were selected for further studies.

The surface of the mild steel specimens immersed in 1.00 M HCl in the absence and presence of 100 ppm of the inhibitors (compounds ***2*** and *7*) at room temperature for 24 h was characterized. The results reveal that the morphological features of the specimen immersed in the electrolyte without the inhibitors (Fig. 2b) suffered severe corrosion attack leading to the formation of pits all over the surface, compared to the freshly polished specimen (Fig. 2a). Corrosion was, however, minimized on the specimens immersed in the electrolyte containing 100 ppm of compound ***2*** (Fig. 2c) and compound *7* (Fig. 2d). This clearly indicates the propensity for adsorption of the molecules on the surface of the metal to form protective films and suppress corrosion attack, as found from the preliminary gravimetric corrosion measurements.

3.2. Effect of concentration and temperature

The corrosion inhibition efficiencies and corrosion rates of the mild steel samples exposed to varying concentrations of ***2*** and *7* (50–500 ppm) are presented in Table 1. As shown in the table, the corrosion inhibition efficiencies of the molecules increased with increasing concentration due to the greater surface coverage of the metal by the molecules. Optimum efficiencies of 90.3% and 96.8% were achieved at 500 ppm and 298 K for ***2*** and *7*, respectively, making *7* an excellent inhibitor of mild steel corrosion in acidic medium. Donor heteroatoms and aromaticity have been identified as key factors that contribute to the corrosion inhibition efficiency of organic molecules (He et al., 2014; Abdulazeez et al., 2019). It is therefore anticipated that compound *7* having more aromatic character and hence greater ability to serve as a donor-center for the empty d orbital of the metal atoms would exhibit greater corrosion inhibition efficiency.

The impact of temperature on the corrosion inhibition efficiency of the molecules was further examined, as presented in Table 1. Increasing the temperature of the solution led to a decrease in the corrosion efficiency of the molecules. This is because at elevated temperatures, the electrostatic force of attraction between the atoms of the metal and adsorbed inhibitor molecules is weakened and the rate of dissolution of the mild steel sample increases. Thus, this result establishes that adsorption of the inhibitor molecules on the surface of the metal occurs mainly through electrostatic attractions (Hamdy and El-Gendy, 2013). With increasing temperature, the corrosion inhibition efficiency of *7* did not change significantly because of its capability for strong adsorption on the surface of the metal, forming a protective inhibitor sheath, which shields the metal from corrosion attack. The results of the temperature studies reveal that molecule *7* exhibits a remarkable inhibition efficiency of 95% at 60 °C (333 K).

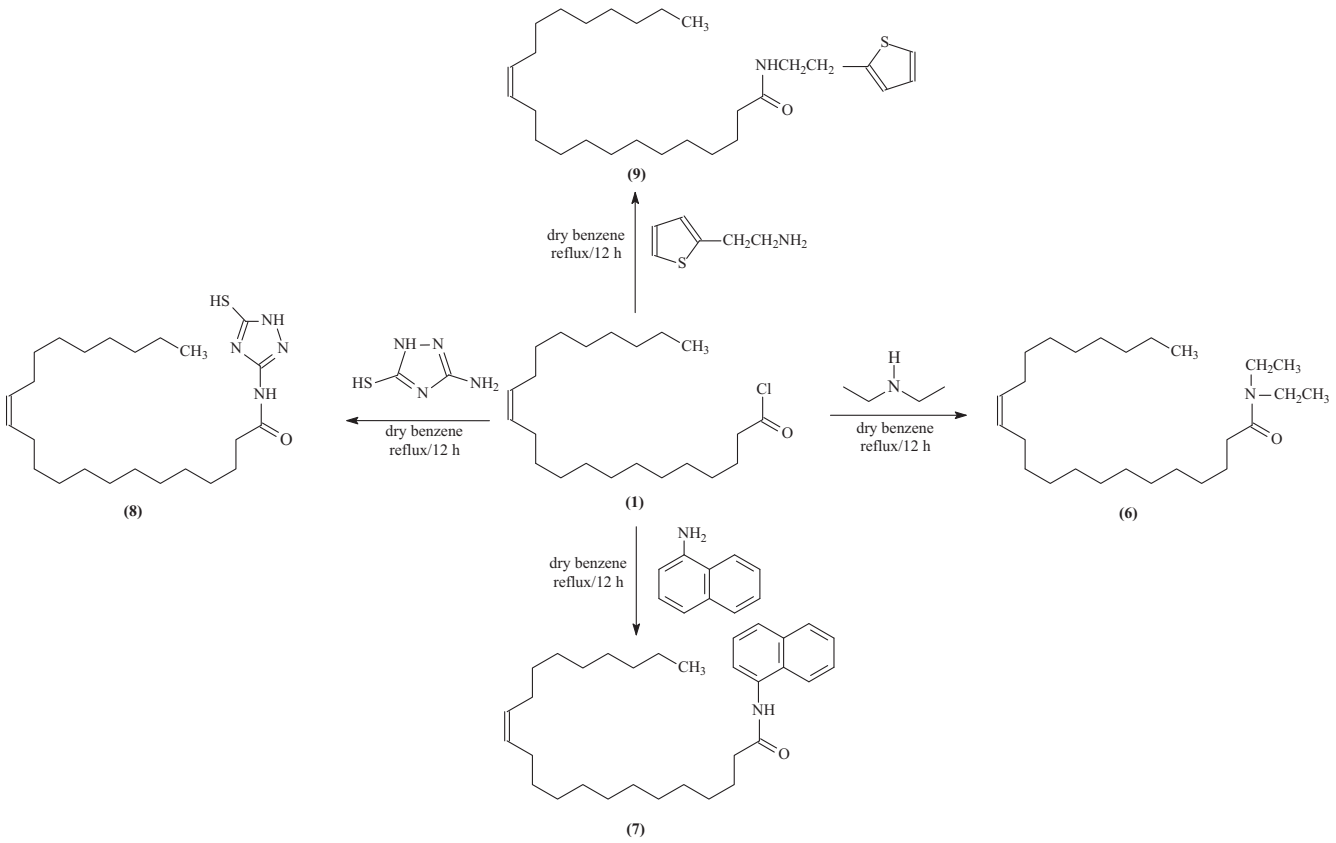

Scheme 3 Schematic diagram of synthesis of acid amide derivatives **(6–9)**.

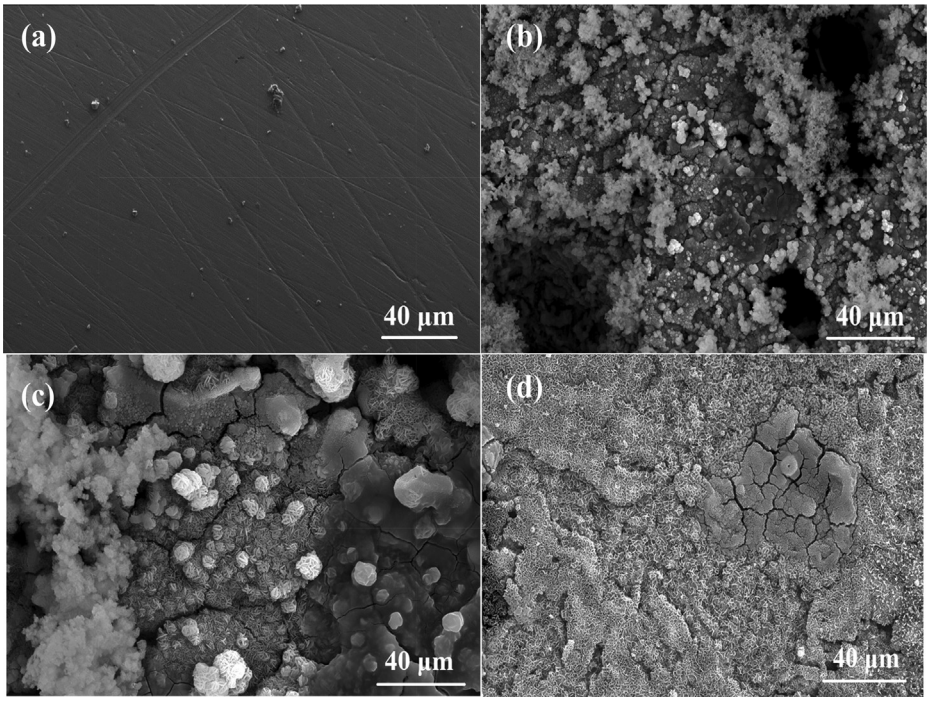

Fig. 2 FESEM micrographs of (a) freshly polished mild steel specimen, (b) specimen immersed in 1.00 M HCl in the absence of inhibitors, (c) specimen immersed in 1.00 M HCl containing 100 ppm of compound **2**, (d) specimen immersed in 1.00 M HCl containing 100 ppm of compound **7**.

Table 1 Weight loss data at different concentrations (50–500 ppm) and temperature (298–333 K).

Inhibitor conc. (ppm)	298 K			313 K			333 K		
	C.R / mmpy	Θ	η%	C.R / mmpy	Θ	η%	C.R / mmpy	Θ	η%
Blank	7.304	–	–	10.50	–	–	15.65	–	–
(2)									
50	3.243	0.556	55.6	5.303	0.495	49.5	8.611	0.450	45.0
100	2.194	0.700	70.0	3.266	0.689	68.9	5.135	0.672	67.2
200	1.767	0.758	75.8	2.730	0.740	74.0	4.305	0.725	72.5
400	0.978	0.866	86.6	1.837	0.825	82.5	3.131	0.800	80.0
500	0.708	0.903	90.3	1.375	0.869	86.9	2.254	0.856	85.6
(7)									
50	2.636	0.639	63.9	3.938	0.625	62.5	6.262	0.600	60.0
100	1.846	0.747	74.7	2.856	0.728	72.8	4.462	0.715	71.5
200	1.322	0.819	81.9	2.047	0.805	80.5	3.256	0.792	79.2
400	0.754	0.896	89.6	1.197	0.886	88.6	1.957	0.875	87.5
500	0.233	0.968	96.8	0.451	0.957	95.7	0.782	0.950	95.0

The interaction between the inhibitor molecules and surface of the metal was further investigated from the adsorption isotherms. Some commonly used adsorption isotherms are the Langmuir, Frumkin, and Temkin isotherms, each of which relates the surface coverage (θ) to the concentration of the inhibitor molecules according to a set of given equations (Ramesh Saliyan and Adhikari, 2008).

The experimental data from the weight loss studies were fitted to the Langmuir adsorption isotherm according to Eq. (4):

$$\frac{C}{\theta} = \frac{1}{K_{ads}} + C \tag{4}$$

where K_{ads} is the adsorption equilibrium constant. A plot C/θ vs. C for molecules ***2*** and *7* (Fig. S1) gave linear fits with slopes of 1.0340, 1.0739, and 1.0846 at 333, 313, and 298 K for ***2*** and 0.9877, 0.9954, and 0.9992 at 313, 298, and 333 K for *7*, respectively. Equation (5) was used to compute the Gibbs free energy of adsorption (Ramesh Saliyan and Adhikari, 2008):

$$\Delta G_{ads} = -RTln(1 \times 10^6 K_{ads}) \tag{5}$$

where 1×10^6 is the water concentration in mg L^{-1}. Typically, ΔG_{ads} values exceeding –40 kJ mol^{-1} are related to chemisorption, while values less than –20 kJ mol^{-1} are generally attributed to physisorption. As shown in Table 2, the ΔG_{ads} values of the molecules are intermediate between those of the two classifications, suggesting that the molecules undergo both chemical and physical adsorption on the surface of mild steel (Ramesh Saliyan and Adhikari, 2008; Luo et al., 2017).

Table 2 Langmuir adsorption data of **2** and **7** at different temperatures.

Inhibitor	Temperature / K	Kads ($\times 10^{-2}$) / $Lmol^{-1}$	ΔG_{ads} / $kJmol^{-1}$
	298	2.27	−24.8
(2)	313	2.13	−25.9
	333	1.89	−27.3
	298	2.71	−25.3
(7)	313	2.56	−26.4
	333	2.38	−27.9

Furthermore, the activation energy for the corrosion of mild steel in 1.00 M HCl in the presence and absence of ***2*** and *7* were computed by applying the Arrhenius equation (Eq. (6)):

$$\log CR = \frac{-E_a}{2.303RT} + \log A \tag{6}$$

where T is the absolute temperature, A is the Arrhenius pre-exponential factor, and R is the ideal gas constant (8.314 J K^{-1} mol^{-1}). A plot of log (CR) against the reciprocal of temperature gave straight lines for both the blank medium and the medium containing the inhibitors, as shown in Fig. 2a and b. The values of E_a obtained from the slopes (Table 3) reveal that the activation energy increased from

Table 3 Activation parameters of mild steel corrosion in the presence of **(2)** and **(7)** molecules.

Medium	E_a / $kJmol^{-1}$	ΔH* / $kJmol^{-1}$	ΔS* / $Jmol^{-1}K^{-1}$
Blank	18.03	37.68	−179.3
(2)			
50	23.38	60.75	−173.8
100	20.15	54.51	−177.1
200	21.34	60.08	−175.8
400	29.61	91.10	−167.1
500	30.06	94.24	−166.8
(7)			
50	20.46	53.84	−176.8
100	21.20	59.20	−176.0
200	21.70	64.05	−175.3
400	22.95	72.99	−173.8
500	26.29	87.88	−171.8

18.03 kJ mol^{-1} for corrosion in the blank medium to 30.06 kJ mol^{-1} and 26.29 kJ mol^{-1} at 500 ppm in the presence of ***2*** and ***7***, respectively. This indicates that addition of the inhibitors reduced the rate of corrosion by increasing in the activation barrier for the dissolution of mild steel. The thermodynamic functions, including the standard entropy of activation (ΔS^*) and the standard enthalpy of activation (ΔH^*) were computed by applying Eq. (7):

$$\log\frac{CR}{T} = \frac{-\Delta H^*}{2.303RT} + \left[\log\frac{R}{Nh} + \frac{\Delta S^*}{2.303R}\right] \quad (7)$$

where N is Avogadro number and h is Planck constant. By plotting log (CR/T) against the reciprocal of the temperature, intercepts [log(R/Nh) + ΔS^*/2.303R] and straight slope lines [$-\Delta H^*$/2.303R] were obtained, as shown in Fig. 3c and d for ***2*** and ***7***, respectively. The results are summarized in Table 3.

The results reveal an increase in the enthalpy of activation (ΔH^*) with an increase in the inhibitor concentration, which suggests that the decrease in the corrosion rate in the presence of the inhibitor molecules is mainly controlled by kinetic parameters (Aljourani et al., 2009). A gradual increase in the entropy of the system (ΔS^*) was also observed upon addition of the inhibitor molecules. This indicates that in the presence of the inhibitors, the disorderliness decreases in the course of transition from the reactants to the activated complex, which is reflected as an overall decrease in the corrosion rate (Abdulazeez et al., 2019) Comparing the inhibitive performance of the studied molecules with those of other reported molecules with similar molecular structures (Table 4) revealed that the molecules performed satisfactorily and could serve as inhibitors of mild steel corrosion in acidic medium (Abdel Hameed et al., 2018; Kannan et al., 2018; Xu et al., 2017; Khanra et al., 2018; Wu et al., 2019; Farhadi et al., 2017; Zhang et al., 2019; Gerengi et al., 2018; Rai et al., 2018; Khalaf et al., 2020; Frisch et al., 2009) (see Table 5).

3.3. Computational results

The lowest energy conformers representing the most stable geometries of the molecules ***2***, ***3***, ***4***, ***5***, ***6***, ***7***, ***8***, and ***9*** are presented in Figs. 4 and 5. According to molecular orbital theory, the degree of interaction between two reacting molecules depends on the distribution and energy levels of their frontier orbitals (Pople and Gordon, 1967). Hence, to understand the underlying mechanistic processes leading to the observed inhibitive properties of the molecules under study, the distribution of the highest occupied molecular orbital (HOMO) and the lowest unoccupied molecular orbital (LUMO), as well as the energy gap maintained between the levels, were inspected. Frontier orbital inspection of the molecules in Figs. 4 and 5 revealed that the HOMO and LUMO orbitals are distributed over the substituents across the amide functional group as well as the respective heteroatoms for all molecules except compounds ***4***, ***5***, and ***6*** for which the HOMO orbitals are

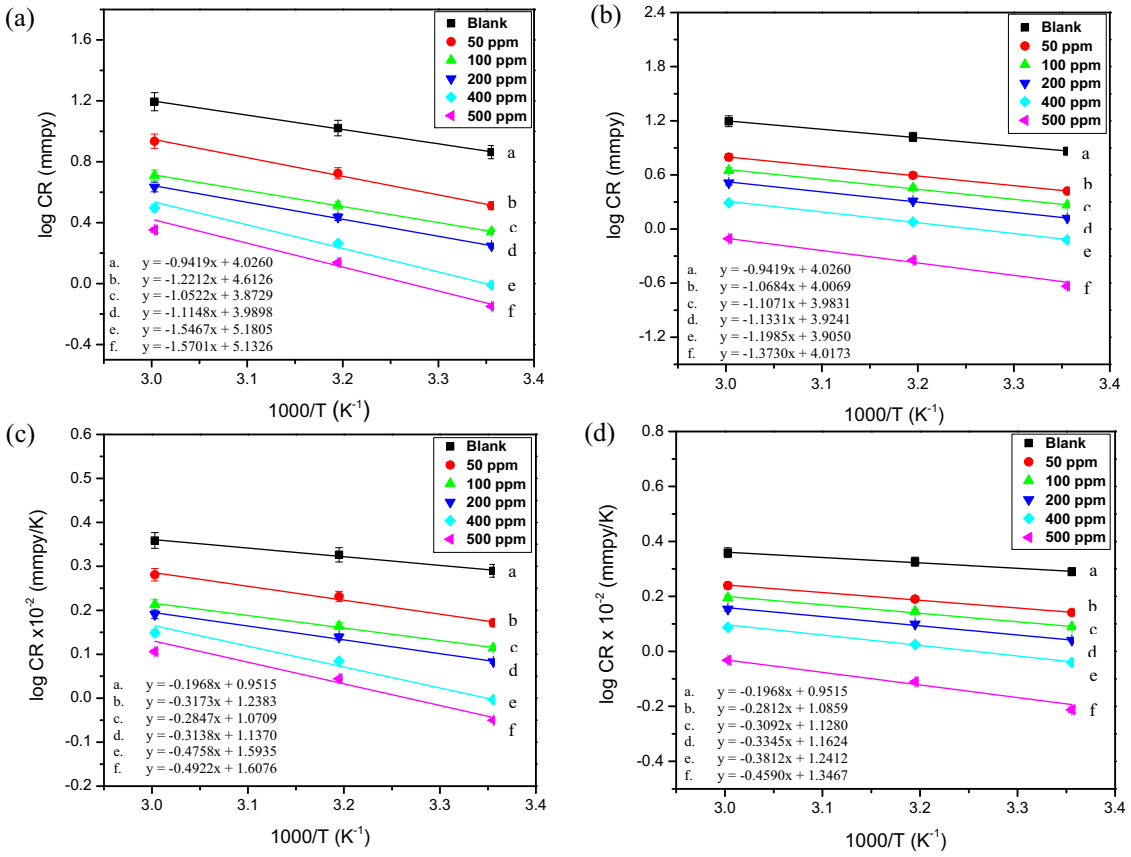

Fig. 3 Arrhenius plots (a, b) and transition state plots (c, d) of mild steel corrosion in 1.00 M HCl in the presence of **(2)** (a, c) and **(7)** (b, d).

Table 4 Comparison of the inhibitive performance with other reported molecules (Abdel Hameed et al., 2018; Kannan et al., 2018; Xu et al., 2017; Khanra et al., 2018; Wu et al., 2019; Farhadi et al., 2017; Zhang et al., 2019; Gerengi et al., 2018; Rai et al., 2018; Khalaf et al., 2020).

Inhibitor	Test medium	Method of evaluation	Metal coupon	IE%	Ref.
Heterocyclic amide derivatives	1.0 M H_2SO_4	Gravimetric, PDP	Carbon steel	95%	(Abdel Hameed et al., 2018)
Carboxamide derivatives	1 N HCl	EIS	Carbon steel	98%	(Kannan et al., 2018)
Fatty acid soap	3.5% NaCl	EIS	Copper	96%	(Xu et al., 2017)
Fatty acid derived from microalgae	1.0 M HCl	Gravimetric, EIS	Mild steel	95%	(Khanra et al., 2018)
Fatty acid derivative	3.5% NaCl	EIS	Mg alloy	–	(Wu et al., 2019)
Fatty acid derivative	3.5% NaCl	PDP	Mg alloy	–	(Farhadi et al., 2017)
Fatty acid derivative	3.5% NaCl	EIS	Copper	99%	(Zhang et al., 2019)
Nitrone-based fatty acid	1.0 M HCl	Gravimetric, PDP, EIS	Steel	95%	(Gerengi et al., 2018)
Fatty acid derived from microalgae	1.0 M HCl	Gravimetric, EIS	Mild steel	96%	(Rai et al., 2018)
Surfactant derived from cooking oil	1.0 M HCl	EIS, PDP	Steel	98%	(Khalaf et al., 2020)
Amides derived from natural fatty acid	1.0 M HCl	Gravimetric	Mild steel	96%	(Present study)

PDP: Potentiodynamic polarization, EIS: Electrochemical impedance spectroscopy.

Table 5 Quantum chemical reactivity descriptors of non-protonated molecules at B3LYP/6-31g(d).

Electronic properties	Compounds							
	(2)	(3)	(4)	(5)	(6)	(7)	(8)	(9)
E_{HOMO} (eV)	−6.10	−6.09	−6.31	−6.31	−6.31	−5.73	−6.25	−6.12
E_{LUMO} (eV)	−0.34	−0.29	0.84	0.85	0.81	−1.17	−0.20	−0.20
ΔE (eV)	5.75	5.79	7.15	7.17	7.12	4.55	6.04	5.91
χ (eV)	3.22	3.19	2.73	2.73	2.75	3.45	3.23	3.16
η (eV)	2.87	2.89	3.57	3.58	3.56	2.27	3.02	2.95
ΔN	0.65	0.65	0.59	0.59	0.59	0.77	0.62	0.64

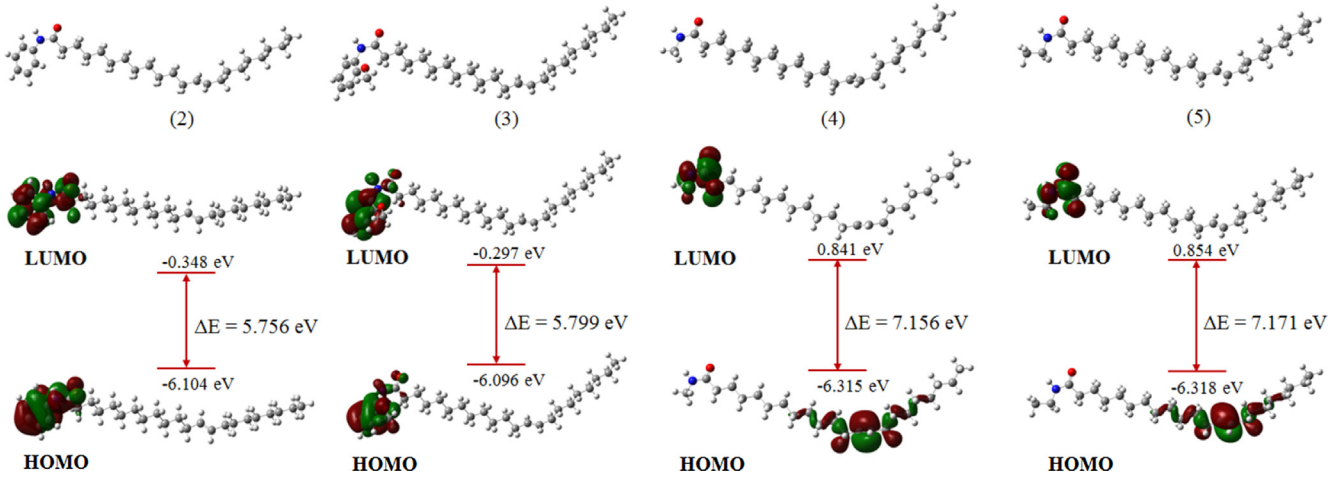

Fig. 4 Optimized geometries and frontier orbital distributions of molecules (2) to (5) at B3LYP/6-31g(d).

distributed over the double-bond present in the aliphatic fragment of the compounds. This reveals the tendency of the molecules to donate charge from the electron-rich centers to the vacant d-orbitals of the metal and their ability to accept back-donation from the atoms of the metal, leading to the formation of strongly adsorbed films that protect the metal from corrosion attack. The HOMO-LUMO energy gap (ΔE) is a measure of the reactivity of a molecule and reveals the charge transfer characteristics of the molecule. It is generally believed that molecules having lower ΔE values exhibit higher charge donation capability and act as better corrosion inhibitors (Abdulazeez et al., 2019). Comparison of the ΔE values of the molecules, summarized in Table 4 (non-protonated molecules) and Table S2 (protonated molecules), shows that molecules ***2*** and *7* having energy gaps of 4.556 and 5.756 eV, respectively, are predicted to possess higher propensity

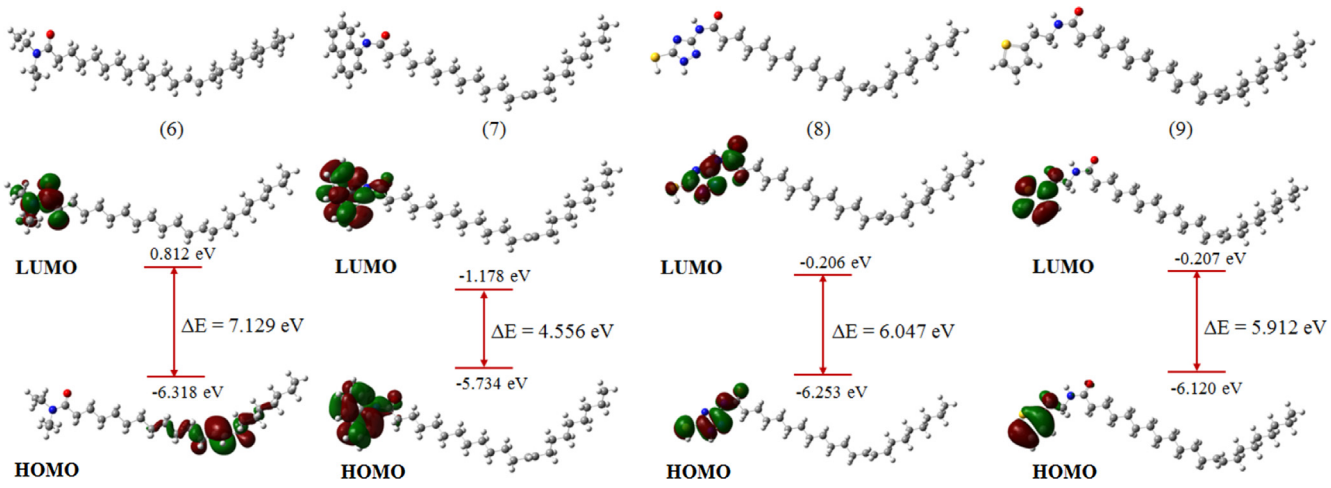

Fig. 5 Optimized geometries and frontier orbital distributions of molecules (6) to (9) at B3LYP/6-31g(d).

towards charge donation to the atoms of the metal and consequently higher corrosion inhibitive tendencies. This is attributed to the presence of aromatic groups on the molecules that serve as centers for electron donation to the metal atoms, in agreement with the results obtained from the gravimetric corrosion measurements. Similar results were obtained for the protonated molecules, as presented in Table S2.

Electronegativity (χ) depicts the electron attracting power of a molecule and is used to indicate the tendency of a given molecule so serve as an effective corrosion inhibitor. In line with the Sanderson's principle of equalization (Sanderson, 1976), molecules having higher electronegativities rapidly attains equalization with atoms of the metal and such molecules exhibits lower corrosion inhibitive performance. However, having higher electronegativity could favor the rapid acceptance of electron back-donation from atoms of the metal leading to higher corrosion inhibitive performance. Hence, comparing χ values among the molecules revealed that molecules ***2*** and *7* having values 3.226 eV and 3.456 eV, respectively could serve as effective inhibitors of mild steel corrosion in acidic medium, in agreement with the experimental data.

The resistance of a given molecule to electron density distortion is measured by its global hardness (η) (Parr et al., 1999, 1991). According to the hard-soft acid-base theory (HSAB) (Geerling and Prof, 2003), molecules having higher η values are mostly less reactive compared to those with lower η values due to their lower propensity to donate charges. Therefore, an effective corrosion inhibitor is the molecule having lower η value in addition to other electronic properties. A closer look at the η values of the molecules (Table 1) revealed that molecule ***2*** and *7* having values of 2.878 eV and 2.278 eV possess higher tendencies to serve as effective inhibitors of mild steel corrosion compared to other molecules, in agreement with the experimental corrosion studies.

ΔN represents the fraction of electrons transferred from the inhibitor molecules to atoms of the metal upon interactions. It is usually used to indicate the direction of flow of electrons between the inhibitors and atoms of the metal. Positive values of ΔN indicates that electron are transferred from the inhibitor molecules to atoms of the metal, while negative values represent the reverse case (Saha, 2015). Comparing values of ΔN of the inhibitor molecules revealed that molecule *7* having higher values of 0.778 in the non-protonated form (Table 4) and 0.696 in the protonated form (Table S2) has the tendency to serve as efficient inhibitors of mild steel corrosion, which agrees with the experimental data. Overall DFT-based quantum chemical calculations yielded results in good agreement with gravimetric corrosion inhibition studies and revealed the significance of aromaticity in the design of highly effective corrosion inhibitors.

4. Conclusion

As corrosion inhibitors, a group of new amide derivatives (13-docosenoic acid amides) was synthesized in high yields (> 90%) from 13-docosenoic acid with primary and secondary aliphatic and aromatic amines, for the first time. The main objective of the study was to synthesize inhibitor molecules from fatty acids that would provide effective protection of mild steel from corrosion in acidic media. The inhibitor having more aromatic character performed better than the aliphatic congener, where the former serves as a donor-center for the empty d-orbitals of the metal atoms and exhibited a higher corrosion inhibition efficiency of 96.8% at 500 ppm. Adsorption of the inhibitor molecules on the surface of mild steel followed the Langmuir adsorption model and the values of the free energy of adsorption (ΔG_{ads}) indicated that the inhibitors are adsorbed on the metal through a mixed physisorption and chemisorption mechanism. The results are indeed very promising and pave the way for exploiting the excellent ability of these amides to inhibit the corrosion of mild steel. Further study has to be carried out to investigate the effectiveness of the inhibitor molecules in acidic media for a longer duration and with flowing systems using additional techniques for corrosion inhibition study.

Author contributions

The manuscript was written through contributions of all authors. All authors have given approval to the final version of the manuscript.

Declaration of Competing Interest

All authors confirmed that there is no any conflict of interest in this article.

Acknowledgements

The authors gratefully acknowledged the financial support provided by Imam Abdulrahman Bin Faisal University through project number 2019-340-Sci. Authors would also like to acknowledge the support received from Dr. Khalid Alhooshani, Head of the Chemistry Department, King Fahd University of Petroleum and Minerals Dhahran, Saudi Arabia.

Appendix A. Supplementary material

Supplementary data to this article can be found online at https://doi.org/10.1016/j.arabjc.2020.03.015.

References

Abdel Hameed, R.S., Alfakeer, M., Abdallah, M., 2018. Inhibiting Properties of Some Heterocyclic Amide Derivatives as Potential Nontoxic Corrosion Inhibitors for Carbon Steel in 1.0 M Sulfuric Acid. Electrochemistry 54, 599.

Abdulazeez, I., Al-Hamouz, O.C., Khaled, M., Al-Saadi, A.A., 2019a. New imidazole-based dimers as potential inhibitors for mild steel corrosion in acidic media: Electrochemical and DFT evaluation. Mater. Corrosion.

Abdulazeez, I., Khaled, M., Al-Saadi, A.A., 2019b. Impact of electron-withdrawing and electron-donating substituents on the corrosion inhibitive properties of benzimidazole derivatives: A quantum chemical study. J. Mol. Struct. 1196, 348–355.

Abdulazeez, I., Zeino, A., Kee, C.W., Al-Saadi, A.A., Khaled, M., Wong, M.W., Al-Sunaidi, A.A., 2019c. Mechanistic studies of the influence of halogen substituents on the corrosion inhibitive efficiency of selected imidazole molecules: A synergistic computational and experimental approach. Appl. Surf. Sci. 471, 494–505.

Ali, S.A., Al-Muallem, H.A., Rahman, S.U., Saeed, M.T., 2008a. Bis-isoxazolidines: A new class of corrosion inhibitors of mild steel in acidic media. Corros. Sci. 50, 3070–3078.

Ali, S.A., Al-Muallem, H.A., Saeed, M.T., Rahman, S.U., 2008b. Hydrophobic-tailed bicycloisoxazolidines: A comparative study of the newly synthesized compounds on the inhibition of mild steel corrosion in hydrochloric and sulfuric acid media. Corros. Sci. 50, 664–675.

Ali, S.A., El-Sharif, A.M., 2012. Novel class of bisquaternary ammonium salts in inhibition of mild steel corrosion in HCl and H_2SO_4. Corros. Eng., Sci. Technol. 47, 265–271.

Ali, S.A., El-Shareef, A.M., Al-Ghamdi, R.F., Saeed, M.T., 2005. The isoxazolidines: the effects of steric factor and hydrophobic chain length on the corrosion inhibition of mild steel in acidic medium. Corros. Sci. 47, 2659–2678.

Ali, S.A., Haladu, S.A., El-Sharif, A.M., 2016a. Diallylbis(3-ethoxy-carbonylpropyl)ammonium chloride: A symmetrically substituted monomer for the synthesis of an alternate zwitterionic-anionic cyclopolymer. Macromol. Res. 24, 163–169.

Ali, S.A., Haladu, S.A., El-Sharif, A.M., 2016b. Synthesis and application of a cyclopolymer bearing a propylphosphonic acid and a propylcarboxylic acid pendants in the same repeating unit. J. Polym. Res. 23, 167.

Ali, S.A., Saeed, M.T., El-Sharif, A.M., 2012a. Diallyl-1,12-diaminododecane-Based Cyclopolymers and Their Use as Inhibitors for Mild Steel Corrosion. Polym. Eng. Sci. 52, 2589–2596.

Ali, S.A., Saeed, M.T., Rahman, S.U., 2003. The isoxazolidines: a new class of corrosion inhibitors of mild steel in acidic medium. Corros. Sci. 45, 253–266.

Ali, S.A., Zaidi, S.M., El-Sharif, A.M., Altaq, A.A., 2012b. Cyclopolymers from N, N-diallyl-N propargyl-(12-N′-formylamino)-1- dodecylammonium chloride and their use as inhibitors for mild steel corrosion. Polym. Bull. 69, 491–507.

Aljourani, J., Raeissi, K., Golozar, M.A., 2009. Benzimidazole and its derivatives as corrosion inhibitors for mild steel in 1M HCl solution. Corros. Sci. 51, 1836–1843.

Antropov, L.I., 1963. The Application of the Potential scale to the Problem of the Corrosion and Protection of Metals. Zh. Fiz. Khim. 37, 965–978.

Aramaki, K., Hagiwara, N., Nishihara, H., 1987. The synergistic effect of anions and the ammonium cation on the inhibition of iron corrosion in acid solution. Corros. Sci. 27, 487–497.

Bahlakeh, G., Dehghani, A., Ramezanzadeh, B., Ramezanzadeh, M., 2019. Highly effective mild steel corrosion inhibition in 1 M HCl solution by novel green aqueous Mustard seed extract: Experimental, electronic-scale DFT and atomic-scale MC/MD explorations. J. Mol. Liq. 293, 111559.

Bentiss, F., Lagrenée, M., Traisnel, M., 2000. 2,5-Bis(n-Pyridyl)-1,3,4-Oxadiazoles as Corrosion Inhibitors for Mild Steel in Acidic Media. Corrosion 56, 733.

Bockris, J.O'M., Yang, B., 1991. The mechanism of corrosion inhibition of iron in acid solution by acetylenic alcohols. J. Electrochem. Soc. 138, 2237.

Cizek, A., 1991. Corrosion Inhibitors used in acidizing. Mater. Perform. 33, 56.

Clewlow, P.J., Haselgrave, J.A., Carruthers, N., 1992. Corrosion inhibitors. EP Patent 0,526,251, A1.

Dehghani, A., Bahlakeh, G., Ramezanzadeh, B., 2019. Green Eucalyptus leaf extract: A potent source of bio-active corrosion inhibitors for mild steel. Bioelectrochemistry 130, 107339.

Dennington, R.K., Millam, T., 2009. J. GaussView, Version 5. Semichem Inc., Shawnee Mission, KS.

Durnie, W., Kinsella, B., De Marco, R., Jefferson, A., 1999. Development of a structure-activity relationship for oil field corrosion inhibitors. J. Electrochem. Soc. 146, 1751.

Farhadi, S.S., Aliofkhazraei, M., Barati Darband, G., Abolhasani, A., Sabour Rouhaghdam, A., 2017. Corrosion and wettability of PEO coatings on magnesium by addition of potassium stearate. J. Magnesium Alloys 5, 210.

Elachouri, M., Kertit, S., Gouttaya, H.M., Nciri, B., Bensouda, Y., Perez, L., Infante, M.R., ElKacemi, K., 2001. Prog. Org. Coat. 43, 267–273.

El-Sharif, A.M., 2017. Effect of organo-nitrogen compounds on inhibition efficiency of mild steel corrosion in acidic media. Asian J. Chem. 29, 1779–1784.

Fedorov, Y.V., Morozova, M.V., 1987. Mechanism of action of combined inhibitors of acid corrosion of metals. Zashch. Met. 23, 758–763.

French, E.C., 1978. Mater. Perform. 37, 20.

Frenier, W.W., Growcock, F.B., 1993. Review on corrosion science and technology. NACE International, Houston, TX, pp. 11–201.

Frenier, W., Growcock, F.B., Lopp, V.R., 1988. A new class of acid corrosion inhibitors. Corrosion 44, 590–598.

Frisch, M.J., et al., 2009. Gaussian 09, Revision B.01, in, Wallingford CT.

Gerengi, H., Solomon, M.M., Öztürk, S., Yıldırım, A., Gee, G., Kaya, E., 2018. Evaluation of the corrosion inhibiting efficacy of a newly synthesized nitrone against St37 steel corrosion in acidic medium: Experimental and theoretical approaches. Mater. Sci. Eng.: C 93, 539.

Growcock, F.B., Frenier, W.W., 1986. Kinetics of Steel Corrosion in Hydrochloric Acid Inhibited with *trans*-Cinnamaldehyde. J. Electrochem. Soc. 104, 86–87.

Hackerman, N., Hurd, R.M., 1962. 1st. Inter. Cong. on Metallic Corrosion. Butterworth, London, p. 166.
Hamdy, A., El-Gendy, N.S., 2013. Thermodynamic, adsorption and electrochemical studies for corrosion inhibition of carbon steel by henna extract in acid medium. Egypt. J. Pet. 22, 17–25.
He, X., Jiang, Y., Li, C., Wang, W., Hou, B., Wu, L., 2014. Inhibition properties and adsorption behavior of imidazole and 2-phenyl-2-imidazoline on AA5052 in 1.00 M HCl solution. Corros. Sci. 83, 124–136.
Kannan, P., Rao, T.S., Rajendran, N., 2018. Improvement in the corrosion resistance of carbon steel in acidic condition using naphthalen-2-ylnaphthalene-2-carboxammide inhibitor. J. Colloid Interface Sci. 512, 618.
Khalaf, M.M., Tantawy, A.H., Soliman, K.A., Abd El-Lateef, H.M., 2020. Cationic gemini-surfactants based on waste cooking oil as new 'green' inhibitors for N80-steel corrosion in sulphuric acid: A combined empirical and theoretical approaches. J. Mol. Struct. 1203, 127442.
Khanra, A., Srivastava, M., Rai, M.P., Prakash, R., 2018. Application of Unsaturated Fatty Acid Molecules Derived from Microalgae toward Mild Steel Corrosion Inhibition in HCl Solution: A Novel Approach for Metal-Inhibitor Association. ACS Omega 3, 12369.
Lorenz, W.J., 1970. Zeitschrift fuer Physikalische Chemie (Leipzig) 244, 65–84.
Luo, H., Guan, Y.C., Khan, K.N., 1998. Corrosion inhibition of a mild steel by aniline and alkylamines in acidic solutions. Corrosion 54, 721–731.
Luo, X., Pan, X., Yuan, S., Du, S., Zhang, C., Liu, Y., 2017. Corrosion inhibition of mild steel in simulated seawater solution by a green eco-friendly mixture of glucomannan (GL) and bisquaternary ammonium salt (BQAS). Corros. Sci. 125, 139–151.
Mernari, B., Elattari, H., Traisnel, M., Bentiss, F., Lagrenee, M., 1998. Inhibiting effects of 3,5-bis(n-pyridyl)-4-amino-1,2,4-triazoles on the corrosion for mild steel in 1 M HCl medium. Corros. Sci. 40, 391–399.
Monroe, R.F., Kucera, C.H., Oates, B.D. 1963. US Patent 3,007,454.
Morad, M., Morvan, J., Pagetti, J., 1995. Proc. 8th Eur. Symp. On Corrosion inhibitors (8 SEIC).
Muralidharan, S., Phani, K.L.N., Pitchumani, S., Ravichandran, S., Iyer, S.V.K., 1995. Polyamino-benzoquinone polymers: a new class of corrosion inhibitors for mild steel. J. Electrochem. Soc. 142, 1478–1483.
Murakawa, T., Hackerman, N., 1964. The double layer capacity at the interface between iron and acid solutions with and without organic materials. Corros. Sci. 4, 387–397.
Osman, M.M., Shalaby, M.N., 2003. Some ethoxylated fatty acids as corrosion inhibitors for low carbon steel in formation water. Mater. Chem. Phys. 77, 261–269.
Parr, R.G., Chattaraj, P.K., 1991. Principle of maximum hardness. J. Am. Chem. Soc. 113 (5), 1854–1855.
Geerling, P., De Prof, F., 2003. Conceptual density functional theory. Chem. Rev. 103, 1793.
Parr, R.G., Szentpály, L.V., Liu, S., 1999. Theoretical Study by Density Functional Theory Method (DFT) of Stability, Tautomerism, Reactivity and Prediction of Acidity of Quinolein-4-One Derivatives. J. Am. Chem. Soc. 121, 1922.
Pople, J.A., Gordon, M., 1967. Molecular orbital theory of the electronic structure of organic compounds. I. Substituent effects and dipole moments. J. Am. Chem. Soc. 89, 4253–4261.
Popova, A., Sokolova, E., Raicheva, S., Chirstov, M., 2003. AC and DC study of the temperature effect on mild steel corrosion in acid media in the presence of benzimidazole derivatives. Corros. Sci. 45, 33–58.
Putilova, I.N., Balezin, S.A., Barannik, V.P., 1960. Metal corrosion inhibitors. Pergamon Press, New York.
Rai, M., Khanra, S., Rai, M., Srivastava, M., Prakash, R., 2018. Pivotal role of levoglucosenone and hexadecanoic acid from microalgae Chlorococcum sp. for corrosion resistance on mild steel: Electrochemical, microstructural and theoretical analysis. J. Mol. Liq. 266, 279.
Ramesh Saliyan, V., Adhikari, A.V., 2008. Inhibition of corrosion of mild steel in acid media by N′-benzylidene-3-(quinolin-4-ylthio) propanohydrazide. Bull. Mater. Sci. 31, 699–711.
Ramezanzadeh, M., Bahlakeh, G., Ramezanzadeh, B., 2019. Study of the synergistic effect of Mangifera indica leaves extract and zinc ions on the mild steel corrosion inhibition in simulated seawater: Computational and electrochemical studies. J. Mol. Liq. 292, 111387.
Rengamani, S., Muralidharan, S., Kulandainathan, M.A., Iyer, S.V., 1994. Inhibiting and accelerating effects of aminophenols on the corrosion and permeation of hydrogen through mild steel in acidic solutions. J. Appl. Electrochem. 24, 355–360.
Revie, R.W., 2000. Uhlig's Corrosion Handbook. John Wiley & Sons, New York.
Revie, R.W., Uhlig, H.H., 2008. Corrosion and corrosion control: an introduction to corrosion science and engineering. Wiley-Interscience, New York.
Rosenfeld, I.L., 1981. Corrosion Inhibitors. McGraw-Hill, New York.
Saha, S.K., Dutta, A., Ghosh, P., Sukul, D., Banerjee, P., 2015. Adsorption and corrosion inhibition effect of Schiff base molecules on the mild steel surface in 1 M HCl medium: a combined experimental and theoretical approach. PCCP 17, 5679–5690.
Sanderson, R., 1976. Chemical Bonds and Bond Energy. Academic Press, New York.
Sanyal, B., 1981. Organic compounds as corrosion inhibitors in different environments-A review. Prog. Org. Coat. 9, 165.
Sastri, V.S., 1998. Corrosion Inhibitors Principles and Applications. John Wiley & Sons, New York.
Sulaiman, K.O., Onawole, A.T., 2016. Quantum chemical evaluation of the corrosion inhibition of novel aromatic hydrazide derivatives on mild steel in hydrochloric acid. Comput. Theor. Chem. 1093, 73–80.
Tabatabaei, M., Asaldous, S., Bahlakeh, G., Ramezanzadeh, B., Ramezanzadeh, M., 2019a. Green method of carbon steel effective corrosion mitigation in 1 M HCl medium protected by Primula vulgaris flower aqueous extract via experimental, atomic-level MC/MD simulation and electronic-level DFT theoretical elucidation. J. Mol. Liq. 284, 658–674.
Tabatabaei, M., Bahlakeh, G., Dehghani, A., Ramezanzadeh, B., Ramezanzadeh, M., 2019b. Combined molecular simulation, DFT computation and electrochemical studies of the mild steel corrosion protection against NaCl solution using aqueous Eucalyptus leaves extract molecules linked with zinc ions. J. Mol. Liq. 294, 111550.
Tabatabaei, M., Ramezanzadeh, M., Ramezanzadeh, B., Bahlakeh, G., 2020. Production of an environmentally stable anti-corrosion film based on Esfand seed extract molecules-metal cations: Integrated experimental and computer modeling approaches. J. Hazard. Mater. 382, 121029.
Tomasi, J., Mennucci, B., Cammi, R., 2005. Quantum Mechanical Continuum Solvation Models. ChemInform 36, 2999–3093.
Uhlig, H.H., Rivie, R.W., 1985. Corrosion and Corrosion Control. John Wiley & Sons, New York.
Yordanov, D., Petkov, P., 2008. J. Univ. Chem. Techno. Metal. 43, 405–408.
Wu, L., Wu, J., Zhang, Z., Zhang, C., Zhang, Y., Tang, A., Li, L., Zhang, G., Zheng, Z., Atrens, A., Pan, F., 2019. Corrosion resistance of fatty acid and fluoroalkylsilane-modified hydrophobic Mg-Al LDH films on anodized magnesium alloy. Appl. Surf. Sci. 487, 569.

Xu, W., Hu, Y., Bao, W., Xie, X., Liu, Y., Song, H., Hao, J., 2017. Appl. Surf. Sci. 399, 491.

Zeino, A., Abdulazeez, I., Khaled, M., Jawich, M.W., Obot, I.B., 2017. Mechanistic study of polyaspartic acid (PASP) as eco-friendly corrosion inhibitor on mild steel in 3% NaCl aerated solution. J. Mol. Liq. 250, 50–62.

Zhang, Z., Li, Z., Hu, Y., Song, A., Xue, Z., Li, Y., Sun, Z., Kong, X., Xu, W., Zhang, S., 2019. Superhydrophobic copper surface fabricated by one-step immersing method in fatty acid salt aqueous solution for excellent anti-corrosion and oil/water separation properties. Appl. Phys. A 125, 558.